X-RAY SPECTROMETRY, VOL. 27, 43–57 (1998)

IntriX: a Numerical Model for Electron Probe Analysis at High Depth Resolution Part I—Theoretical Description

P.-F. Staub*
Laboratoire de Chimie Physique–Matière et Rayonnement, Université Paris VI, 11 rue P. et M. Curie, 75231 Paris cedex 05, and CAMECA, 103 Bd St-Denis, 92403 Courbevoie cedex, France

The theoretical description of a quantitative electron probe model, IntriX, is presented. It consists of a numerical reconstruction of the in-depth ionization distribution $\Phi(\rho z)$ through the use of basic physical macroscopic parameters describing the electron beam–matter interaction. With the aim of characterizing nanometer features in samples, specific attention is paid to the treatment of analysis performed on in-depth non-homogeneous samples (films on substrates) and also at low beam energies E_0 ($E_0 < 5$ keV) and near the ionization threshold E_c ($E_0/E_c < 2$). © **1998 John Wiley & Sons, Ltd.**

X-Ray Spectrom. **27**, 43–57 (1998)

INTRODUCTION

The quantitative analysis of solid materials by the so-called electron probe (EP) method consists in bombarding a sample with monokinetic electrons (incident energy E_0) in order to ionize the core levels (binding energy E_c) of atoms inside the target and to interpret, by means of an appropriate model, the measured intensity of characteristic signal (x-rays or Auger electrons) emitted by these atoms during their deexcitation. Since the pioneering work by Castaing and Descamps,[1] many models have been proposed which basically intend to reproduce the ionization depth distribution $\Phi(\rho z)$ inside the analyzed sample. In cases of bulk homogeneous samples, this has become a routine task and is now fairly well completed by a number of programs,[2–4] where $\Phi(\rho z)$ distributions are represented by easily computable analytical functions; these analytical models are primarily parameterized by fitting experimental and Monte Carlo $\Phi(\rho z)$ data concerning homogeneous standard samples.

As a result of the increasing technological interest in layered materials, adapting the EP models to the quantitative study of non-uniform samples has become critical. Valuable methodological information for applying $\Phi(\rho z)$ models to stratified samples can be found in works by Pouchou and Pichoir[5] and Bastin *et al.*[6] The basic configuration of such systems is an emitting film F deposited on a substrate S: one has to determine $\Phi(\rho z)$ in F by taking into account the electron backscattering properties of S. In fact, most analytical models are not suited to a realistic description of $\Phi(\rho z)$, particularly when F and S have significantly different atomic numbers. In this case, 20–30% errors can arise in film thickness determination.[5] This failure is due to the fact that analytical models treat F–S systems as 'averaged' homogeneous samples, by means of most often physically meaningless weighting laws applied to their parameters. In addition, expectations are based on Monte Carlo simulations,[7,8] with which any sample configurations can, in principle, be investigated. However, other problems arise with Monte Carlo methods due to their complexity, statistical character and cost in terms of computing time, the latter excluding at present their use as routine analytical tools.

An intermediate relevant solution was proposed by August and Wernisch,[9] which takes the form of a semi-empirical numerical model operating on macroscopic and generally well known electronic scattering parameters such as electron transmission and backscattering coefficients, the corresponding energy and angular distributions and the ionization cross-section. This method combines non-statistical and quick computational properties of semi-empirical models with the adaptability and physical relevance allowed by numerical (non-analytical) treatments. The reliability of such an electron scattering model in the case of F–S systems has already benefited some applications,[10] and is promising for extended developments.

In its principle, the EP quantitation model described in the present paper, and entitled IntriX, approaches the treatment adopted by August and Wernisch.[9] The most important difference between the two models is that the program developed by August and Wernisch is mainly devoted to the interpretation of intensity measurements performed in the field of 'classical' electron probe analysis, i.e. for incident energies $E_0 \geqslant 6$ keV and overvoltages $U_0 = E_0/E_c > 1.7$ (E_c is the ionization threshold for the considered X transition), whereas for IntriX we paid an extra attention to analysis at low energies

* Correspondence to: P.-F. Staub, CAMECA, 103 Bd St-Denis, 92403 Courbevoie cedex, France.
Contract/grant sponsor: Ministère Français de la Recherche et de l'Enseignement Supérieur.

CCC 0049–8246/98/010043–15 $17.50

Received 9 April 1996
Accepted 1 April 1997

($0.5 \leqslant E_0 \leqslant 5$ keV) and at low overvoltages ($1 \leqslant U_0 \leqslant 2$). Moreover, we have generalized our model to the case of emitting materials buried under coating films. The interest in performing EP analysis in these last ranges of conditions, and the usefulness of a new quantitation model adapted to them (IntriX), are now considered.

There is an increasing need for characterizing compositionally, dimensionally and chemically thinner and thinner structures, from 1 nm to hundreds of nm, such as superficial segregations or interfacial regions in layered materials. This involves performing EP analysis with better and better depth resolution, i.e. making the emitting thickness inside the sample coincide best with the thin zone of interest. This is achieved by lowering the incident energy E_0 so that the primary electrons reach the zone to be excited with energies exceeding the threshold E_c by a small quantity δE ranging from tens to a few hundred eV, the energy δE then being entirely dissipated during the short crossing of the investigated zone. To balance the subsequent narrowness of the emitting thickness, it is important to maximize the counting rate through the use of overvoltages U_0 as large as possible. This last condition is achieved by taking E_c values as small as possible. Consequently, soft x-ray lines ($E_c \leqslant 4$–5 keV) are preferred to harder ones and this explains why high depth resolution EP analysis require incident energies $E_0 = E_c + \delta E$ typically lower than 5 keV. Furthermore, for a given emitting thickness, low-energy EP investigations benefit from strong peak-to-background ratios (usually one or two orders of magnitude greater than when using classical incident energies), and generally suffer from much less x-ray self-absorption, owing to shallower excitation depths.

Another advantage of the EP technique performed at low energies is the possibility of obtaining information about the chemical state of emitting species inside the target. Indeed, if detected by a spectrometer of sufficient spectral resolution (typically better than 10^{-3}), the shape of soft x-ray lines can be interpreted in terms of valence band occupancy, and then related to the emitting atoms chemical bonds. This method, performed at very low overvoltages ($U_0 \leqslant 1.5$), has been successfully applied to the characterization of nanometer interfacial regions in various layered structures,[11] and can be associated advantageously with an adapted quantitative EP model such as IntriX.

Developing accurate low-energy EP techniques is also advantageous for determining very light elements (Be, B, C, N, O). Indeed, owing to the strong absorption of their x-ray lines inside the sample, optimizing intensity acquisition for these elements requires shallow excitations, which is best achieved at low energies (typically 5–15 keV for bulk samples, often less for layered structures).

Finally, restricting the electron penetration to small depths is of strong interest for obtaining high-resolution x-ray images in EP microanalysis techniques,[12] provided a good electron optical column is used to ensure a small lateral size of the incident beam. These images can become very powerful analytical tools if reliably quantified.

All quantitative EP models that have been developed to date have to overcome increased uncertainty when applied to low-energy and low-overvoltage analysis. The various reasons for this can be summarized as follows:

(1) Concerning low energies ($E_0 \leqslant 5$ keV), only very few measured $\Phi(\rho z)$ curves exist (eight at $E_0 = 5$ keV,[13,14] three at 4 keV[13] and none below), thus limiting seriously the database upon which analytical models are established. Moreover, it is often difficult to compensate this lack of data by means of fitting the trends indicated by Monte Carlo calculations since, at low energies, the latter require particularly complex programs and long computing times to provide sufficiently accurate results.[15,16] These theoretical difficulties originate from the failure of the Born approximation in the treatment of the interaction between primary and atomic electrons having similar energies. Consequently, this prohibits the direct use of easy to handle formalisms such as the Rutherford approach for angular scattering and the Bethe approach for energy losses when it is intended to extend the reliability of classical EP models from the high-energy towards the low-energy region. However, more sophisticated models using have been developed recently,[17–19] considering single scattering events and using the Mott cross-section for elastic scattering or the modified Grizinski cross-section for inelastic collisions; these models extend the applicability of Monte Carlo technique to the incident energy range 2–5 keV.

Finally, it is worth noting that some assumptions are often made in the classical models with regard to the constancy of certain parameters versus E_0 (as for the backscattering coefficient) that fail for low energies, owing to the drastic changes in scattering cross-sections that occur in this region.[20]

(2) Concerning low overvoltages ($1 < U_0 < 2$), the main problems are related to the ionization cross-section Q. First, near the ionization threshold, Q values are not well determined either theoretically (again because Born's approximation fails) or experimentally and the simple empirical equations usually encountered in EP models are not reliable.[21] Second, because Q exhibits a strong growth with overvoltage $U = E/E_c$ up to $U \approx 2$, the ionizing capabilities of primary electrons traveling in the sample with nearly identical energies E ($E < 2E_c$) may be very different. As a result, the more electrons having energies close to E_c, i.e. the smaller is U_0, the more approximations ruling the energy dependence of electronic parameters are expected to lose their relevance. This important fact affects some fundamental approximations used in all classical analytical EP models, such as the 'average energy loss approximation.' In latter, the penetrating electron beam is considered as monoenergetic all along its path, its energy being set equal to the mean energy E_m of the actually energy spread electron beam. This approximation clearly fails for near-threshold interactions: owing to the strong variation of Q, the simple computation of $Q(E_m)$ is not sufficient to account for the whole beam ionization probability; in fact, as noted by Murata and Sugiyama[7] for their Monte Carlo simulations, one should always include the energy straggling of primary electrons when computations are made for low overvoltages. Other approximations usually encountered in classical analytical EP models are also expected to produce low overvoltage aberrations, such as those used to represent

more or less crudely the energy distribution of backscattered electrons. Finally, as explained in the following, enhancements of the beam angular scattering associated with low energy loss electron–atom collisions have to be taken into account specifically when near-threshold analyses are performed.

All these difficulties, added to those concerning the treatment of non-homogeneous samples, strongly question the setting up of a high depth resolution EP routine technique via the use of classical analytical or Monte Carlo means. The proposed numerical model IntriX has been built up in order to avoid these difficulties. IntriX is structured on electronic parameters which have been adjusted to reliable experimental data collected at incident energies as low as 0.5 keV; this should guarantee good performance in the low-energy region. The numerical procedure adopted allows us to take into account the energy dispersion of primary electrons, a necessary step to cope with the case of low overvoltage analysis. Finally, IntriX benefits from a computational celerity similar to August and Wernisch's model[9] as regards the treatment of layered samples.

In the present paper, except for indicated cases, all energies are given in keV, angles in degrees and mass depths in $\mu g\ cm^{-2}$.

PHYSICAL RECONSTRUCTION OF THE IONIZATION DEPTH DISTRIBUTION: THE IntriX MODEL

The proposed model accounts for the core ionizations caused by primary electrons when passing through an elementary layer dz situated at depth z inside the target. The situation is pictured in Fig. 1. Ionization by the electrons that are transmitted through the depth z and which are crossing dz for the first time is labeled $i = 1$. Order $i = 2$ is associated with electrons backscattered beyond depth z, then crossing dz for the second time,

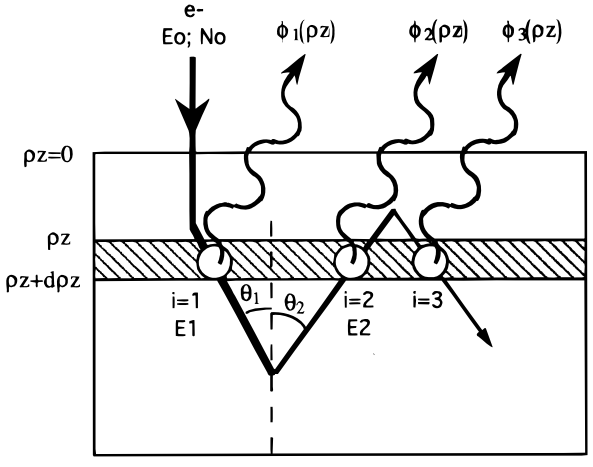

Figure 1. IntriX's schematic representation of the beam scattering inside the sample: contributions $\phi_i(\rho z)$ to ionization of the layer $d\rho z$ are labeled with respect to the number of times i that the ionizing electrons have passed through it. E_i and θ_i denote, respectively, the energy and the deflection from the surface normal of i-order electrons at mass depth ρz.

and so on. In the present work, we shall neglect orders $i > 3$, assuming that the electrons concerned are not numerous or energetic enough to produce a significant contribution to the ionization.

The total ionization depth distribution function Φ is conventionally given in units of mass depth (ρz, where ρ is the sample density) and normalized to the number of ionizations ${\phi_1}^0$ (per mass depth unit) produced in an isolated layer $d\rho z$ in which the effects of electron scattering can be ignored:

$$\Phi(\rho z) = \frac{\phi(\rho z)}{{\phi_1}^0} = \frac{1}{{\phi_1}^0} \sum_{i=1}^{3} \phi_i(\rho z) = \sum_{i=1}^{3} \Phi_i(\rho z) \qquad (1)$$

with

$$ {\phi_1}^0 = \frac{c}{A} N_0 Q(U_0) \qquad [\text{mol cm}^2\ \text{g}^{-1}] \qquad (2)$$

where c and A are, respectively, the weight fraction and the atomic mass of emitting atoms in the sample, N_0 is the number of incident electrons, $Q(U)$ is the electro-ionization cross-section of the core level involved in the detected emission and $U = E/E_c$ is the overvoltage and is defined as the ratio between the energy E of the ionizing electron and E_c. The $\Phi_i(\rho z)$ and $\phi_i(\rho z)$ functions are, respectively, the normalized and non-normalized contributions to ionization of the i-order electrons at mass depth ρz inside the target; the following three sections are dedicated to their determination.

Calculation of the first-order contribution $\Phi_1(\rho z)$ (transmitted electrons)

The contribution of the electrons which are transmitted with energies between E_1 and $E_1 + dE_1$ through the layer ρz, $\rho z + d\rho z$ can be written as

$$d\phi_1(\rho z) = \left\langle \frac{1}{\cos\theta} \right\rangle_1^{E_1 \geqslant E_c} \frac{c}{A} N_0\, g_t(E_0, E_1, \rho z)\, dE_1 Q(U_1) \qquad (3)$$

with $U_1 = E_1/E_c$.

$g_t(E_0, E_1, \rho z)$ denotes the energy distribution of the electron beam when transmitted through a mass thickness ρz. Details concerning the computation of g_t can be found in Appendix 1. $(1/\cos\theta)_1^{E_1 \geqslant E_c}$ is a factor ($\geqslant 1$) which accounts for the angular distribution of all the *efficient* electrons ($E_1 \geqslant E_c$) transmitted in mass depth ρz, i.e. after penetration of $d\rho z$ (see Fig. 1). It reflects the mean increase of the electron travel for an oblique crossing of $d\rho z$ compared with a straight crossing and will be called the 'elongation factor.' See Appendix 1 for a detailed computation of this factor.

Once integrated over the efficient energy spectrum, the first-order contribution can be written as follows:

$$\Phi_1(\rho z) = \frac{1}{{\phi_1}^0} \int_{E_c}^{E_0} \frac{d\phi_1(\rho z)}{dE_1} dE_1 \qquad (4)$$

$$= \frac{1}{Q(U_0)} \left\langle \frac{1}{\cos\theta}(E_0, \rho z) \right\rangle_1^{E_1 \geqslant E_c} \times \int_{E_c}^{E_0} g_t(E_0, E_1, \rho z) Q(U_1)\, dE_1 \qquad (5)$$

Calculation of the second-order contribution $\Phi_2(\rho z)$ (backscattered electrons)

Using the basic relationships (1) and (2), the second-order surface contribution can be written as follows:

$$\phi_2(0) = {\phi_1}^0 \Phi_2(0) = \frac{c}{A} N_0 Q(U_0)[\Phi(0) - \Phi_1(0) - \Phi_3(0)]$$

Considering besides that, by definition, we have $\Phi_1(0) = 1$ and $\Phi_3(0) = 0$, we obtain

$$\phi_2(0) = \frac{c}{A} N_0 Q(U_0)[\Phi(0) - 1] \tag{6}$$

Let us define the parameter R as follows:

$$R = \Phi(0) - 1 = \Phi_2(0) \tag{7}$$

This quantity reflects the contribution of backwards electrons to surface ionization; it has been shown by different workers[22–25] that $\Phi(0)$, and hence R, could be satisfactorily expressed as a function of the sample backscattering coefficient η and the incident overvoltage U_0:

$$R = R(\eta, U_0)$$

A new analytical expression for R adapted in cases of low overvoltages is proposed in Appendix 2.

By analogy with Eqn (6), if we now consider the second-order contribution produced at mass depth $\rho z > 0$ inside the target (see Fig. 1), due to the $\mathrm{d}N_t = N_0 g_t(E_1)\ \mathrm{d}E_1$ electrons transmitted through the mass thickness ρz with an energy E_1, $E_1 + \mathrm{d}E_1$, we can write

$$\mathrm{d}\phi_2(\rho z) = \frac{c}{A} N_0 g_t(E_0, E_1, \rho z)\ \mathrm{d}E_1 Q(U_1) R(\eta_{\theta_1}, U_1) \tag{8}$$

where η_θ denotes the backscattering coefficient of an electron beam impinging on a sample with an incidence angle θ; we have already proposed a quantitation for this parameter.[26] We introduce it in order to account for the increase of the backscattering at mass depth ρz as the first-order angular scattering is growing. The effective incident angle θ_1 is taken so that

$$\frac{1}{\cos\theta_1} = \left\langle \frac{1}{\cos\theta}(\rho z) \right\rangle_1^{E_1 \geqslant E_c} \tag{9}$$

In view of Eqn (3), Eqn (8) can be rewritten as

$$\frac{\mathrm{d}\phi_2(\rho z)}{\mathrm{d}E_1} = \frac{\mathrm{d}\phi_1(\rho z)}{\mathrm{d}E_1} R(\eta_{\theta_1}, U_1) \Big/ \left\langle \frac{1}{\cos\theta} \right\rangle_1^{E_1 \geqslant E_c} \tag{10}$$

and then

$$\Phi_2(\rho z) = \frac{1}{{\phi_1}^0} \frac{1}{\langle 1/\cos\theta \rangle_1^{E_1 \geqslant E_c}} \times \int_{E_c}^{E_0} \frac{\mathrm{d}\phi_1(\rho z)}{\mathrm{d}E_1} R(\eta_{\theta_1}, U_1)\ \mathrm{d}E_1 \tag{11}$$

Calculation of the third-order contribution ($i = 3$)

The elementary third-order contribution can be deduced from the second-order contribution in the same way as we deduced the second-order from the first-order contribution, i.e. using at one upper i-order the analogue of Eqn (10):

$$\frac{\mathrm{d}^2\phi_3(\rho z)}{\mathrm{d}E_1\,\mathrm{d}E_2} = \frac{\mathrm{d}^2\phi_2(\rho z)}{\mathrm{d}E_1\,\mathrm{d}E_2} R[\eta_{\theta_2}(\rho z), U_2] \Big/ \left\langle \frac{1}{\cos\theta} \right\rangle_2^{E_2 \geqslant E_c} \tag{12}$$

where $\eta_{\theta_2}(\rho z)$ is the backscattering coefficient of the layer of mass thickness ρz from which third-order electrons are returning (cf. Fig. 1). In IntriX, this quantity is estimated following the method proposed by Sogard,[27] but modified in order to match the low-energy data given by Vyatskin *et al.*[28] Details about these modifications can be found in a thesis by Staub.[29]

$\langle 1/\cos\theta \rangle_2^{E_2 \geqslant E_c}$ is the elongation factor that reflects the mean angular scattering through the surface layer of those second order electrons having an energy $E_2 \geqslant E_c$. See Appendix 2 for a detailed computation of this factor.

From Eqn (12), the exact evaluation of the $\phi_3(\rho z)$ would involve a double integration over energy, at the cost of a significant loss ot time through computations. However, as in most cases the third-order electrons contribute to less than 15% of the total ionization (if $U_0 \leqslant 10$), simplifying statements can be assumed to estimate it without producing any important errors in the total predicted signal. Along this line, we consider the second-order electrons as a monoenergetic beam, effective energy E_2^{eff}, impinging back on the layer ρz, $\rho z + \mathrm{d}\rho z$ with an effective incidence angle θ_2^{eff}. Thus, the second-order derivative in Eqn (12) is suppressed and we meet an integration analogous to Eqn (11):

$$\Phi_3(\rho z) = \frac{1}{{\phi_1}^0} \frac{1}{\langle 1/\cos\theta \rangle_2^{E_2 \geqslant E_c}} \times \int_{E_c}^{E_0} \frac{\mathrm{d}\phi_2(\rho z)}{\mathrm{d}E_1} R[\eta_{\theta_2 \mathrm{eff}}(\rho z), U_2^{\mathrm{eff}}]\ \mathrm{d}E_1 \tag{13}$$

with $U_2^{\mathrm{eff}} = E_2^{\mathrm{eff}}/E_c$. Introducing Eqn (10), we obtain

$$\Phi_3(\rho z) = \frac{1}{{\phi_1}^0} \frac{1}{\langle 1/\cos\theta \rangle_2^{E_2 \geqslant E_c} \langle 1/\cos\theta \rangle_1^{E_1 \geqslant E_c}} \times \int_{E_c}^{E_0} \frac{\mathrm{d}\phi_1(\rho z)}{\mathrm{d}E_1} R(\eta_{\theta_1}, U_1) R[\eta_{\theta_2 \mathrm{eff}}(\rho z), U_2^{\mathrm{eff}}]\ \mathrm{d}E_1 \tag{14}$$

Consistent with the method used at first order [cf. Eqn (9)], the effective angle θ_2^{eff} is chosen so that

$$\frac{1}{\cos\theta_2^{\mathrm{eff}}} = \left\langle \frac{1}{\cos\theta} \right\rangle_2^{E_2 \geqslant E_c} \tag{15}$$

To a first approximation, the effective energy E_2^{eff} can be taken as equal to the mean energy $\overline{E_2}$ of the second-order electrons. $\overline{E_2}$ can be expressed as an empirical function of the incident energy E_1 and backscattering coefficient η_{θ_1} in the following way:[30]

$$E_2^{\mathrm{eff}} = \overline{E_2} \approx E_1 \frac{1 + \eta_{\theta_1}}{2} \tag{16}$$

As explained in Appendix 2, the approximation $E_2^{\mathrm{eff}} = \overline{E_2}$, which is identical with that used by

Cazaux,[24] definitely fails as the applied overvoltage is decreasing ($U_1 < 3$). Nevertheless, as the third-order contribution is at the same time becoming negligible, the error produced is not critical. Otherwise, a more exact treatment of the E_2^{eff} estimate, not detailed here but including the effect of threshold proximity, can be found elsewhere.[29]

General expression for the total ionization depth distribution $\Phi(\rho z)$

Summing the three orders of contribution to ionization given by Eqns (4), (11) and (14), we finally obtain

$$\Phi(\rho z) = \sum_{i=1}^{3} \Phi_i(\rho z) = \frac{1}{(c/A)N_0\, Q(U_0)} \times \int_{E_c}^{E_0} \frac{\mathrm{d}\phi_1(\rho z)}{\mathrm{d}E_1} \left\{1 + \frac{R(\eta_{\theta_1}, U_1)}{\langle 1/\cos\theta \rangle_1^{E_1 \geq E_c}} \times \left[1 + \frac{R[\eta_{\theta_2{}^{\text{eff}}}(\rho z), U_2^{\text{eff}}]}{\langle 1/\cos\theta \rangle_2^{E_2 \geq E_c}}\right]\right\} \mathrm{d}E_1 \qquad (17)$$

where $\mathrm{d}\phi_1(\rho z)$ is given by Eqn (3). As can be seen, although it accounts for the three first i orders, Eqn (17) requires only one numerical integration to be computed.

Figure 2 displays an example of a $\Phi(\rho z)$ distribution computed with Eqn (17), showing the different i order contributions to ionization of the Si K level in a silver matrix at $E_0 = 10$ keV. This type of graph allows an interesting physical insight into what actually occurs during the beam–matter interaction. For instance, in that particular case, one can note the importance of high-order electrons ($i = 2$ and 3), related to the strong backscattering probability in such a high-Z matrix. In particular, the third-order contribution increases sharply after the surface, thus influencing significantly the mass depth at which the $\Phi(\rho z)$ curve exhibits its maximum.

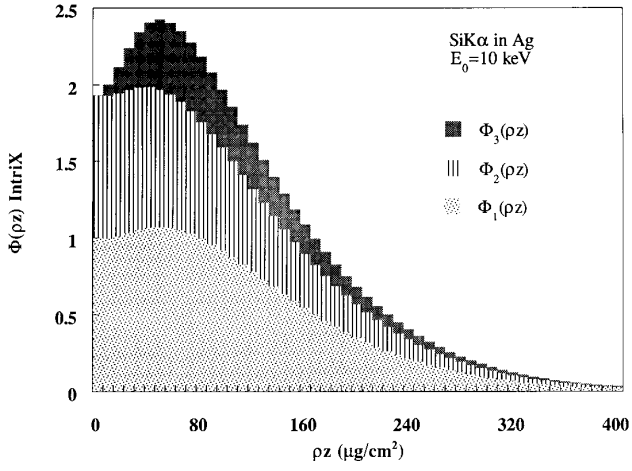

Figure 2. Comprehensive diagram showing the contributions of the three interaction orders ($i = 1$, 2, 3) to the K level ionization function $\Phi(\rho z)$ of an Si tracer embedded in Ag matrix, as computed by IntriX ($E_0 = 10$ keV).

Accounting for the effect of the fluorescence from the continuum

Core ionization is not only caused by beam electrons but also by bremsstrahlung photons ($h\nu > E_c$) generated in the sample (continuum fluorescence). As explained in Appendix 2, the fluorescence contribution $\phi_F(0)$ to ionizations occurring in an elementary surface layer $\mathrm{d}\rho z$ can be linked, as a first approach, to the corresponding second-order contribution $\phi_2(0)$ by means of the following relation:

$$\phi_F(0) = \phi_2(0)\mathcal{F}(\eta, U_0) \qquad (18)$$

where the function $\mathcal{F}$ can be approximated by the analytical expression (A23).

Analogous to Eqn (18), the fluorescence contribution to a layer $\mathrm{d}\rho z$ situated at mass depth $\rho z > 0$ due to bremsstrahlung photons generated in the target by electrons impinging on $\mathrm{d}\rho z$ with energy E_1, $E_1 + \mathrm{d}E_1$ will be estimated as follows:

$$\mathrm{d}\phi_F(\rho z) = \mathrm{d}\phi_2(\rho z)\mathcal{F}(\eta, U_1) \qquad (19)$$

The total fluorescence contribution $\Phi_F(\rho z)$ is then computed by integrating Eqn (19) between E_c and E_0.

This treatment is approximate and accounts only partly for the bremsstrahlung fluorescence at mass depth ρz. Indeed, the $\mathcal{F}$ factor, originally a surface parameter, is defined from experiments in which only backwards photons (i.e. those returning to the surface layer) are contributing to intensity. This is no longer the case when the emitting layer is significantly buried, since ionizing photons can be generated above this layer. For ionization threshold energies lower than 5 keV, which are the interesting cases for performing high depth resolution electron probe microanalysis (EPMA), the continuum fluorescence never exceeds a few per cent of the total emitted intensity,[31–33] so that the induced error is not expected to be critical. However, for higher energy EPMA, it has been shown that continuum fluorescence can become important, especially for high atomic number matrices.[32] In these cases, an improvement to IntriX would consist in applying a rigorous calculation of the fluorescence, similar to that proposed by Pfeiffer *et al.*,[32] which is also based on an electron scattering model.

Photoionization induced by characteristic lines (characteristic fluorescence) is not considered here, although it could become important, at least in particular cases, especially for a stratified specimen.[33] As for continuum fluorescence, the probability of secondary characteristic fluorescence is expected to decrease strongly when considering low excitation energies.[33,34]

Studying different types of configurations for the beam–sample interactions

Non-coated emitting samples. The general scheme for this type of sample corresponds to the case of either an emitting film on a substrate or a semi-infinite homogeneous sample (a film whose mass thickness ρz_f exceeds the maximum electron penetrating depth).

A film–substrate (F–S) system can be considered as composed of an emitting film of mass thickness $\rho D =$

$\rho z_f - \rho z$ covering the substrate; it is illustrated in Fig. 3. In this case, first-order electrons impinge on a different stratified system at each mass depth ρz. As a consequence, the presence of a substrate of a different nature than the emitting film primarily affects the second-order contribution through a change in the backscattering coefficient η_{θ_1} according to ρz. The ionization depth function is computed using Eqn (17), but replacing the bulk coefficient η by a film–substrate coefficient η^{F-S} for which various equations have been proposed.[35–37] In the frame of the present work, we use the following expression proposed by De Nee:[38]

$$\eta^{F-S} = \eta^S + (1 - \eta^S/\eta^F)\eta^F(\rho D) \quad (20)$$

Coated emitting materials. Let us suppose that the emitting part of the sample is now covered by a coating material Z' of mass thickness $\rho' z'$. Electrons transmitted at the interface are spread both energetically [energy distribution $g'_t(E_0, E'_1, \rho' z')$] and spatially (effective incident angle θ'_1). Owing to this non-normal incidence at the interface $z = 0$, electrons transmitted at depth z have crossed statistically a longer path than they would if they had been issued from a normal incidence beam. In Fig. 4, this longer path is illustrated by a curved trajectory, whose length is expressed by the curvilinear coordinate $\zeta(z)$. We evaluate this effective length $\zeta(z)$ by dividing the emitting thickness into two separate zones, as follows:

—*a transient zone*, where electrons gradually lose the memory of their incident (interface) angle until they reach a complete diffusion depth, denoted $z_D^{\theta_1}$. The effective length $\zeta(z)$ of the transmitted electrons path in this region has to satisfy the following boundary condition:

$$\left(\frac{\partial \zeta}{\partial z}\right)_{z=0} = \frac{1}{\cos \theta'_1} \quad (21)$$

In this transient zone, the g_t and $\langle 1/\cos\theta \rangle_1^{E_1 \geq E_c}$ functions are computed by introducing the backscattering coefficient $\eta_{\theta_1'}$ (instead of η for normal incidence).

As the diffusion angle θ'_1 never exceeds 45° (see Appendix 1), the electron projected path to reach complete diffusion depth is simply approximated to $z_D^{\theta_1'}/\cos\theta'_1$; by analogy with the case of normal incidence, this path is computed by setting it equal to X_{E_c} (see Appendix 1).

—*a complete diffusion zone*, for $z \geq z_D^{\theta_1'}$, in which effects of the interface incidence angle are neglected: the situation becomes equivalent to normal incidence (see above), i.e. additional path lengths are projected along the z axis. This can be written as

$$\left(\frac{\partial \zeta}{\partial z}\right)_{z \geq z_D^{\theta 1'}} = 1$$

Consistently, the g_t and $\langle 1/\cos\theta \rangle_1^{E_1 \geq E_c}$ functions are computed using the normal incidence backscattering coefficient η.

Gathering these hypotheses, we propose the following expression for $\zeta(z)$, which meets the preceding conditions and produces physically consistent results:[39]

$$\zeta = \frac{z}{\cos \theta'_1}\,[1 - f_{\theta_1'}(z)]$$

with

$$f_{\theta_1'}(z) = \frac{1 - \cos\theta'_1}{2}\,\frac{z}{z_D^{\theta_1'}}$$

in the transient zone and

$$\zeta = \zeta(z_D^{\theta_1'}) + z - z_D^{\theta_1'}$$

in the complete diffusion zone.

Because ζ is greater than z, more inelastic events are involved in the case of non-normal incidence, thus widening the energy distribution $g_t^{\theta_1'}$ at depth z as compared with the distribution g_t issuing from a normal incidence beam. To account for this effect, $g_t^{\theta_1'}$ at depth z is taken equal to g_t at depth $\zeta(z)$; this is written as

$$g_t^{\theta_1'}(E'_1, E_1, \rho z) = g_t(E'_1, E_1, \rho\zeta)$$

Once integrated over the interface energy spectrum g'_t, the first-order contribution, as derived from Eqn (3), finally becomes

$$d\phi_1(\rho z) = \frac{c}{A} N_0 Q(U_1)\, dE_1 \times \int_{E_c}^{E_0} \left\langle \frac{1}{\cos\theta}(E'_1, \rho\zeta + \rho z_{eq.}) \right\rangle_1^{E_1 \geq E_c} \times g'_t(E_0, E'_1, \rho' z') g_t(E'_1, E_1, \rho\zeta)\, dE'_1 \quad (22)$$

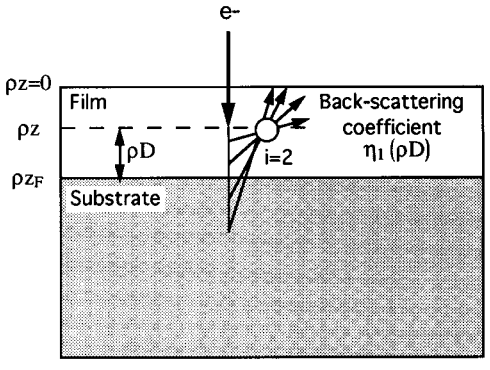

Figure 3. General case of an emitting film on a substrate. Illustration of the fact that the distance D from interface has an effect on the backscattering coefficient η_1 inside the film.

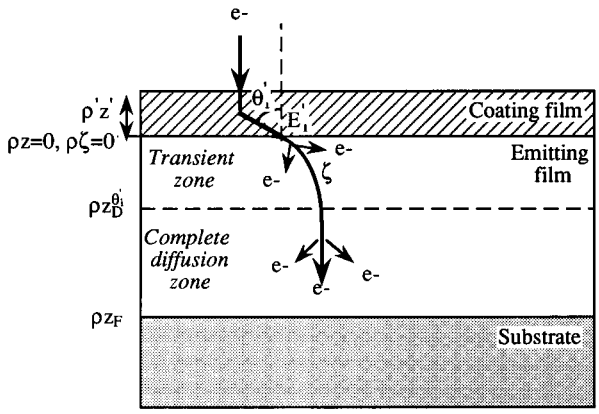

Figure 4. Transmission of electrons in an emitting substrate covered by a coating film of depth z'. The curved trajectory illustrates the effective path length ζ crossed by transmitted electrons at depth z under the interface, after having been deflected with a mean angle θ'_1. The complete diffusion depth $z_D^{\theta_1'}$ separates the transient zone ($0 \leqslant z \leqslant z_D^{\theta_1'}$) from the complete diffusion zone ($z > z_D^{\theta_1'}$).

where $\rho z_{eq.}$ is the thickness of the emitting material that would have produced the same state of first-order angular diffusion as the coating film (see Appendix 1). Contributions of superior interaction orders ($i = 2$ and 3) are obtained from the first-order interaction following the same procedure as described above for homogeneous samples.

CONCLUSION

Classical EPMA models are all founded on an *analytical* formulation of $\Phi(\rho z)$. With the increase in computer speed, the need for such formal calculations has become less crucial and more physical meaning can be incorporated into models, with the aim of analyzing more complex samples with better accuracy. Along this line, IntriX involves *numerical* integration to generate $\Phi(\rho z)$ functions. It operates on empirically pre-settled macroscopic parameters that keep good physical consistency for incident energies ranging from tens of keV down as low as 0.5 keV. The computing time is considerably reduced compared with Monte Carlo codes [typically a few seconds to compute a $\Phi(\rho z)$ function with a regular workstation], thus making possible its use as a routine analysis tool.

The ability of IntriX to match existing measurements over a very wide range of physical conditions, and consequently the relevance of using it as a reliable high depth resolution electron probe model, are described elsewhere.[39]

Acknowledgements

The author thanks Professor C. Bonnelle, Dr F. Vergand and Dr P. Jonnard for useful discussions. The author is also grateful to Professor R. Castaing for having agreed to supervise the doctoral thesis dedicated to this work. This work was supported by the Ministère Français de la Recherche et de l'Enseignement Supérieur.

REFERENCES

1. R. Castaing and J. Descamps, *J. Phys.* (*Paris*) **16**, 304 (1955).
2. J. L. Pouchou and F. Pichoir, in *11th Conference on X-Ray Optics and Microanalysis* (*London, Ontario, 1986*), edited by J. D. Brown and R. Packwood, 1987, p. 247.
3. R. H. Packwood and J. D. Brown, *X-Ray Spectrom.* **10**, 138, (1981).
4. C. Merlet, *Mikrochim. Acta* **114/115**, 363 (1994).
5. J. L. Pouchou and F. Pichoir, *Scanning Microsc. Suppl.* **7**, 167 (1993).
6. G. F. Bastin, J. M. Dijkstra, H. J. M. Heijligers and D. Klepper, *Microbeam Anal.* **2**, 29 (1993).
7. N. Amman and P. Karduck, in *Microbeam Analysis*, edited by J. R. Michael and P. Ingram, p. 150. San Francisco Press, San Francisco (1990).
8. K. Murata and K. Sugiyama, *J. Appl. Phys.* **66**, 4456 (1989).
9. H. J. August and J. Wernisch, *X-Ray Spectrom.* **20**, 131 (1991).
10. C. Schiebl, L. Foster, A. Pfeiffer and A. Testoni, in *Proceedings of the 28th Annual MAS Meeting*, edited by J. J. Friel, New Orleans, LA, 1994, p. 199.
11. T. P. Nguyen, P. Jonnard, F. Vergand, P.-F. Staub, J. Thirion, M. Lapkowski and V. H. Tran, *Synth. Met.* **75**, 175 (1995).
12. J. Ruste, *EDF Report, HT-41/INTE 1644-A*, EDF (1993).
13. W. Rehbach, Doctoral Thesis, Aachen (1988).
14. D. A. Sewell, G. Love and V. D. Scott, *J. Phys. D* **18**, 1233 (1985).
15. K. Murata, H. Kotera and K. Nagami, *J. Appl. Phys.* **54**, 1110 (1983).
16. P. Karduck and W. Rehbach, in *Electron Probe Quantitation*, edited by K. F. J. Heinrich and D. E. Newbury, p. 191. Plenum Press, New York (1991).
17. L. Reimer, *Mikrochim. Acta* (*Suppl.*) **13**, 1 (1996).
18. X. Llovet, A. Riveros and F. Salvat, *Mikrochim. Acta* (*Suppl.*) **13**, 409 (1996).
19. R. Gauvin, P. Hovington and D. Drouin, *Scanning* **17**, 202 (1995).
20. H. J. Fitting, C. Hinkfoth, H. Glaefeke and J. C. Kuhr, *Phys. Status Solidi A* **126**, 85 (1991).
21. C. J. Powell, *Ultramicroscopy*. **28**, 24 (1989).
22. W. Reuter, in *6th ICXOM*, edited by G. Shinoda, K. Kohra and T. Ichinokawa, p. 121. University of Tokyo Press, Tokyo (1972).
23. H. J. August and J. Wernisch, *Scanning* **12**, 14 (1990).
24. J. Cazaux, *Microsc. Microanal. Microstruct.* **3**, 1 (1992).
25. J. L. Pouchou and F. Pichoir, in *11th Conference on X-Ray Optics and Microanalysis* (*London, Ontario, 1986*), edited by J. D. Brown and R. Packwood, 1987, p. 247.
26. P.-F. Staub, *J. Phys. D* **27**, 1533 (1994).
27. M. R. Sogard, *J. Appl. Phys.* **51**, 4417 (1980).
28. A. Y. Vyatskin, V. V. Trunev and H. J. Fitting, *Radio Eng. Electron. Phys.* **18**, 1238 (1973).
29. P.-F. Staub, Doctoral Thesis, Université P. et M. Curie, Paris (1995).
30. H. J. Fitting, *J. Phys. D* **8**, 1480 (1975).
31. M. Green, PhD Thesis, University of Cambridge (1962).
32. A. Pfeiffer, C. Schiebl and J. Wernisch, *X-Ray Spectrom.* **25**, 131 (1996).
33. J. L. Pouchou and F. Pichoir, *Scanning* **12**, 212 (1990).
34. J. L. Pouchou, *Mikrochim. Acta.* (*Suppl.*) **13**, 39 (1996).
35. H. Niedrig, *J. Appl. Phys.* **53**, R15 (1982).
36. R. H. Packwood and G. Rémond, *Scanning Microsc.* **6**, 367 (1992).
37. S. V. Kazakov, S. G. Konnikov and V. V. Tretyakov, *X-Ray Spectrom.* **19**, 269 (1990).
38. P. B. De Nee, in *Proceedings on Scanning Electron Microscopy* Vol. I, p. 741. SEM, AMF O'Hare, IL (1978).
39. P.-F. Staub, P. Jonnard, F. Vergand, J. Thirion and C. Bonnelle, *X-Ray Spectrom.* **27**, 58 (1998).

APPENDIX 1: QUANTIFYING THE PHYSICAL PARAMETERS TO COMPUTE THE FIRST ORDER CONTRIBUTION TO IONIZATION ($i = 1$)

The energetic distribution of transmitted electrons g_t

An analytical expression has already been proposed[A1] for the energetic distribution of transmitted electrons g_t, which depends only on two basic parameters, as follows:

—*the electron projected range*, X_0, which corresponds to the mean sample thickness for which the number of transmitted electrons is attenuated with a factor 1/e. In the frame of the present work, the following estimate of

X_0 will be used, which is very close to one proposed previously:[A1]

$$\frac{\rho X_0}{\mu g\ cm^{-2}} = \frac{5.9}{n}\left(\frac{E_0}{keV}\right)^n \quad (A1)$$

where the energy-range exponent n depends on E_0 as proposed by Kanaya and Kawakatsu.[A2]

As evidenced in a paper by Staub *et al.*,[39] the precision with which the parameter X_0 is known directly affects the determination of the emitting thickness in stratified samples with the model IntriX.

—*the bulk backscattering coefficient*, η, giving the number N_b of incident electrons that are returning in the half-space of incidence after having interacted with the specimen: $\eta = N_b/N_0$.

It should be noted that the analytical expressions used in the IntriX program to quantify X_0 and η have been chosen because they are fitted on data acquired at energies as low as 0.5 keV;[26,A1] this is necessary to ensure the reliability of IntriX in the low-energy region ($E_0 < 5$ keV).

The elongation factor of transmitted electrons $\langle 1/\cos\theta\rangle_1^{E_1 \geqslant E_c}$

As no theoretical formulation or empirical fit exists to describe the elongation factor with confidence, most workers generally make the implicit approximation that the angular scattering does not depend on electron energy E_1; this can be summarized as follows:

$$\left\langle \frac{1}{\cos\theta} \right\rangle_1^{E_1 \geqslant E_c} = \left\langle \frac{1}{\cos\theta} \right\rangle_1^{E_1 \geqslant 0} \quad (A2)$$

Although approximation (A2) produces acceptable results in the general case, it fails when the applied overvoltages are weak ($E_1 < 2E_c$), as illustrated by Staub *et al.*[39] The following is devoted to the setting up of a more realistic estimate of the elongation factor.

The total elongation factor ($E_1 \geqslant 0$). As already demonstrated by Reuter,[22] the total elongation factor can be obtained from the angular distribution $G_t^{E_1 \geqslant 0}(\theta, \rho z)$ of an electron beam transmitted through a film of mass thickness ρz:

$$\left\langle \frac{1}{\cos\theta}(\rho z) \right\rangle_1^{E_1 \geqslant 0} = \frac{\int_0^{\pi/2} G_t^{E_1 \geqslant 0}(\theta, \rho z) 2\pi \sin\theta\, d\theta/\cos\theta}{\int_0^{\pi/2} G_t^{E_1 \geqslant 0}(\theta, \rho z) 2\pi \sin\theta\, d\theta} \quad (A3)$$

A number of experimental studies have addressed the determination of G_t functions[A3–A6] for various ranges of mass thickness ρz, incident energy E_0 and atomic number Z. From experimental data at high energies ($E_0 > 50$ keV), Soum *et al.*[A6] derived a simple law that synthesizes all their results concerning the G_t functions, in the form of a Gaussian distribution:

$$G_t^{E_1 \geqslant 0}(\theta)/G_t^{E_1 \geqslant 0}(0) = \exp[-V^2(\rho z)] \quad (A4)$$

with

$$V^2 = \frac{\theta^2}{2\theta_p^{E_1 \geqslant 0}(\rho z)\tan\theta_p^{E_1 \geqslant 0}(\rho z)}$$

where $\theta_p^{E_1 \geqslant 0}$, called the most probable diffusion angle, is the value of θ that maximizes the function $G_t(\theta)\sin\theta$. Equation (A4) is illustrated in Fig. A1 (thick curves), where ratios $G_t(\theta)/G_t(0)$ are reproduced for different values of $\theta_p^{E_1 \geqslant 0}(\rho z)$. Soum *et al.*[A6] observed that, for a given E_0, θ_p increases with mass thickness ρz, until it reaches a saturation value $\theta_p \approx 37°$ at a critical mass thickness ρz_D, called the complete diffusion mass depth. Beyond ρz_D, the $G_t(\theta)$ function undergoes no further change.

The disadvantage of the Gaussian form in Eqn (A4) is that it is not realistic for high diffusion angles; indeed, it gives $G_t(\pi/2) \neq 0$, then producing an infinite value for the elongation factor when the numerator integral of Eqn (A3) is calculated. With the aim of finding a more realistic description of $G_t(\theta)$ over the whole angular range $0 \leqslant \theta \leqslant \pi/2$, we propose the following simple representation:

$$G_t^{E_1 \geqslant 0}(\theta)/G_t^{E_1 \geqslant 0}(0) = (\cos\theta)^{\tau(\theta_p E_1 \geqslant 0)} \quad (A5)$$

with

$$\tau = \frac{0.283}{(1-\cos\theta_p^{E_1 \geqslant 0})^{1.125}} \quad (A6)$$

The good agreement between this description and those proposed by Soum *et al.*[A6] is illustrated in Fig. A1. In addition to the fact that the physical condition $G_t(\pi/2) = 0$ is actually achieved, the $G_t(\theta)$ functions proposed here allow an analytical calculation of Eqn (A3), leading to the simple equation

$$\left\langle \frac{1}{\cos\theta} \right\rangle_1^{E_1 \geqslant 0} = 1 + \frac{1}{\tau(\theta_p^{E_1 \geqslant 0})} \quad (A7)$$

Reaching the complete diffusion region, i.e. for $\theta_p = \theta_{pmax} \approx 37°$, Eqn (A6) gives $\tau \approx 2$, thus leading to an angular distribution in $\cos^2\theta$. This behavior was predicted theoretically by Bothe,[A7] and has also been confirmed experimentally for lower energies ($5 \leqslant E_0 \leqslant 20$ keV) by Cosslett and Thomas.[A4] For the lowest energies to be considered here ($0.5 \leqslant E_0 < 5$ keV), slight deviations from the Bothe law have been experimentally evidenced by different workers,[A3–A6] the saturation distribution tends toward a cosine distribution (i.e. $\tau = 1$), which is associated with $\theta_{pmax} = 45°$. Nevertheless, one can note that Eqns (A5) and (A6) keep their validity in the complete diffusion region even for these low energies since actually we have $\tau(45°) \approx 1$. In this respect, we shall assume that the representation in Eqn (A5) remains valid for energies as low as 0.5 keV.

Experimental values of $\theta_p^{E_1 \geqslant 0}$ (E_0, ρz) for extended ranges of incident energy ($5 \leqslant E_0 < 20$ keV) and atomic number ($13 \leqslant Z < 79$) have been published by Cosslett and Thomas.[A4] They found that the dependence of θ_p on Z decreases as E_0 is lowered from 20 to 5 keV; at 5 keV this dependence almost completely vanishes.

With the aim of finding universal law giving $\theta_p^{E_1 \geqslant 0}$, we have represented the data of Cosslett and Thomas as function of the 'reduced diffusion mass depth' $\rho z/\rho z_D(E_0)$ rather than as functions of the two indepen-

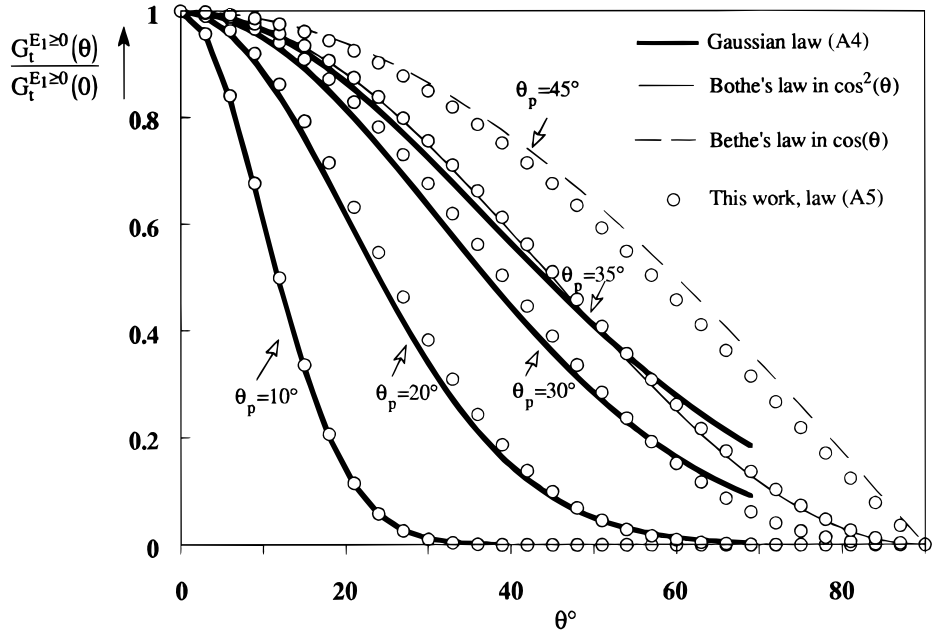

Figure A1. Normalized angular distributions of transmitted electrons for different values of the most probable diffusion angle θ_p. Comparison of the semi-empirical Gaussian fit in Eqn (A4) by Soum *et al.*[A6] with the proposed cosine power function (A5). Theoretical complete diffusion distributions in cos θ and cos^2 θ, associated with low and high incident energies, respectively, are also represented.

dent quantities E_0 and ρz. We estimate $z_D(E_0)$ using the definition already adopted by Kanaya and Kawakatsu,[A2] according to which the complete diffusion depth is reached when the transmission fraction is 1/e. This is then simply written as

$$z_D = X_0 \Rightarrow \frac{\rho z}{\rho z_D} = \frac{\rho z}{\rho X_0}$$

A good general agreement with the data of Cosslett and Thomas[A4] is reached using the following interpolation law (see Fig. A2):

$$\theta_p^{E_1 \geq 0}(E_0, \rho z) \equiv \theta_p^{E_1 \geq 0}\left(\frac{\rho z}{\rho X_0}\right) \approx \theta_{pmax}\left\{1 - \exp\left[-\left(2.24 + 6.05 \times 10^{-3} \times \left(\frac{E_0}{\ln \eta}\right)^2\right)\frac{\rho z}{\rho X_0}\right]\right\} \quad \text{(A8)}$$

We noticed that the data collected by Cosslett and Thomas did not allow one to reproduce satisfactorily the experimental $\Phi(\rho z)$ curves in A1 matrices: the variation of measured $\theta_p^{E_1 \geq 0}$ with depth always seemed too slow. August and Wernisch[9] came to the same conclusion when trying to apply these measurements for building their own model. The adjustment we made to correct these discrepancies explains why, in Fig. A2, a stronger deviation of our Eqn (A8) to the experimental data can be observed for A1 at 20 keV as compared with other elements.

Below 5 keV, as the E_0-dependent term in Eqn (A8) becomes negligible, $\theta_p^{E_1 \geq 0}(\rho z/\rho X_0)$ functions are nearly identical with those displayed in Fig. A2 for 5 keV, and they coincide for all Z.

The partial path elongation factor ($E_1 \geq E_c$). For a given $E_c \geq 0$, we now exclusively consider the efficient electrons, i.e. those which are transmitted with an energy $E_1 \geq E_c$. It was shown experimentally by Vyatskin and Khramov[A8] that the relative number N_1/N_0 of these electrons which are transmitted through a thin film (mass depth ρz) can be represented by the law

$$\frac{N_1(\rho z)}{N_0} = \exp\left[-\left(\frac{\rho z}{\rho X_{E_c}}\right)^{p(\eta, E_c)}\right] \quad \text{(A9)}$$

where X_{E_c} is a projected range analogous to $X_0 = X_{E_c} = 0$, but restricted to efficient electrons, and p is a parameter which reflects the efficiency ratio of elastic to inelastic processes inside the material.

From Eqn (A9), at a given E_0 and for $E_c = 0$, the beam transmission behavior is completely determined by X_0 and η; this is consistent with the fact that both of these parameters are sufficient to describe the value of $\theta_p^{E_1 \geq 0}$ as given by Eqn (A8). More generally, the facts that both the parameterization and the functional shape of Eqn (A9) are maintained whatever the value of $E_c \geq 0$ indicates that the transmission behavior of a part of the beam having an energy $E_1 \geq E_c$ can be treated analogously to the previous singular case $E_c = 0$, but as if occurring in a fictitious material characterized by the parameters X_{E_c} and $p(\eta, E_c)$. Using the approximation $p(\eta, E_c) = p(\eta, 0)$, which has already been discussed in a previous paper,[A1] the most probable scattering angle associated with energies $E_1 \geq E_c$ can be predicted simply by applying this analogy to Eqn (A8), as follows:

$$\theta_p^{E_1 \geq E_c}(E_0, \rho z) \equiv \theta_p^{E_1 \geq E_c}\left(\frac{\rho z}{\rho X_{E_c}}\right) \approx \theta_{pmax}\left\{1 - \exp\left[-\left(2.24 + 6.05 \times 10^{-3} \times \left(\frac{E_0}{\ln \eta}\right)^2\right)\frac{\rho z}{\rho X_{E_c}}\right]\right\} \quad \text{(A10)}$$

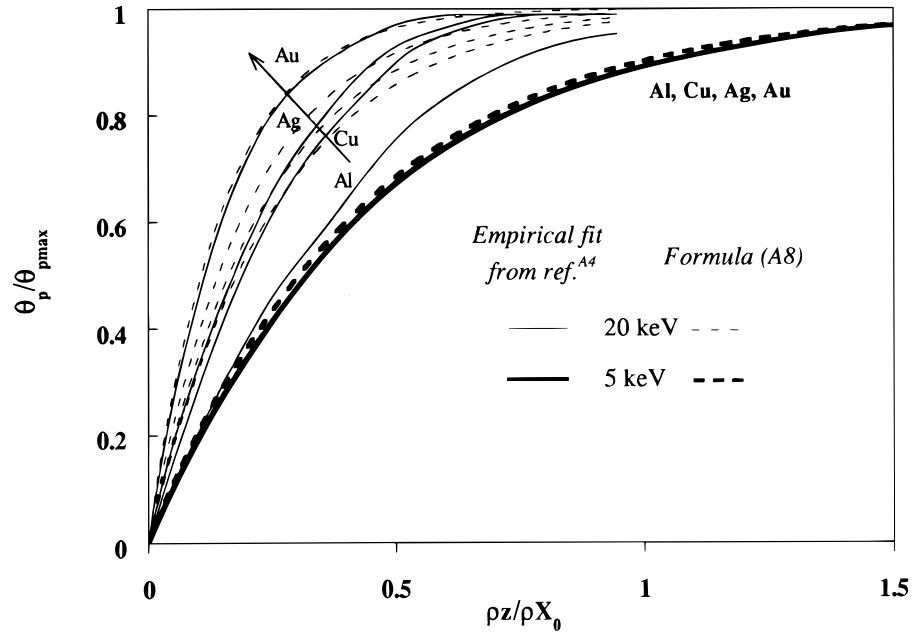

Figure A2. Comparison between experimental data from Cosslett and Thomas[A4] Eqn (A9) for the most probable diffusion angle θ_p as a function of the reduced thickness $\rho z/\rho X_0$, for various atomic numbers ($Z = 13$, 29, 47 and 79) and incident energies ($E_0 = 5$ and 20 keV).

For a given E_0 in a given matrix, because $X_{E_c} \leqslant X_0$, the behavior of $\theta_0^{E_1 \geqslant E_c}$ as described by Eqn (A10) consists in a shallower angular diffusion as E_c is increased, i.e. as the overvoltage is reduced. Statistically, this is easily understandable considering that lowering the overvoltage is equivalent to restricting the accounted electrons to a more and more elastically scattered part of the transmitted beam and that, in fact, these electrons are those which contribute the most severely to the angular widening of the whole beam.

The projected range X_{E_c} is evaluated using the classical continuous slowing down approximation for the beam energy, in which the range of E_0 electrons is the range to reach the energy E_c complemented by that of electrons having an initial energy E_c; this is written as

$$X_0(E_0) = X_{E_c}(E_0) + X_0(E_c)$$

thus giving rise to

$$X_{E_c}(E_0) = X_0(E_0) - X_0(E_c) \tag{A11}$$

and, in view of Eqn (A1):

$$\rho X_{E_c}(E_0) = \rho X_0(E_0)\left[1 - \left(\frac{E_c}{E_0}\right)^n\right] = \frac{5.9}{n}(E_0^n - E_c^n) \tag{A12}$$

Along the same line, the partial path elongation factor is calculated analogously to the total one [see Eqn (A7)], i.e.

$$\left\langle \frac{1}{\cos\theta} \right\rangle_1^{E_1 \geqslant E_c} = 1 + \frac{1}{\tau(\theta_p^{E_1 \geqslant E_c})} \tag{A13}$$

APPENDIX 2: QUANTIFYING THE PHYSICAL PARAMETERS TO COMPUTE THE SECOND ORDER CONTRIBUTION TO IONIZATION ($i = 2$)

The elongation factor of backwards electrons $\langle 1/\cos\theta \rangle_2^{E_2 \geqslant E_c}$

As for the case of first-order electrons (see Appendix 1), the elongation factor of second-order electrons $\langle 1/\cos\theta \rangle_2^{E_2 \geqslant E_c}$ is not conveniently available from theory or experiments, so that one always applies for backscattered electrons the same non-energy dependent approximation as Eqn (A2). Moreover, as it is known from several experiments[A6,A9,A10] that the total angular spectrum $G_b(\theta)$ of backscattered electrons follows a cosine distribution ($\tau = 1$), thus giving rise, by use of Eqn (A9), to an elongation factor of 2, approximation (A2) applied to second-order electrons becomes

$$\left\langle \frac{1}{\cos\theta} \right\rangle_2^{E_2 \geqslant E_c} = \left\langle \frac{1}{\cos\theta} \right\rangle_2^{E_2 \geqslant 0} = 2 \tag{A14}$$

The fact that backscattered angular distributions are actually energy dependent has been experimentally evidenced by Darlington,[A11] who showed that there is a shift of the measured $g_b(E_2)$ spectra towards higher energies as the detection is lowered near grazing angles (see Fig. 4 in Darlington's paper). A simple physical description for this phenomenon can be found in Niedrig[35] (see Fig. 16 in Niedrig's paper), where it is shown how electrons being backscattered by single

elastic processes (Rutherford scattering) exhibit much flatter angular distributions than the cosine distribution to be expected when all backscattered electrons are considered together, leading to a value of the elongation factor of >2. This point is of importance since the present study includes near-threshold analysis in which only the most energetic electrons, i.e. those which have been significantly scattered by single elastic processes, are contributing to the signal intensity. In these latter cases, approximation (A14) is consequently expected to be irrelevant.

$\langle 1/\cos\theta \rangle_2^{E_2 \geq E_c}$ can be linked to the surface second-order contribution $\Phi_2(0)$ using an equation analogous to Eqn (5), but now applied to backscattered electrons:

$$\Phi_2(0) = \frac{1}{Q(U_0)} \left\langle \frac{1}{\cos\theta} \right\rangle_2^{E_2 \geq E_c} \times \int_{E_c}^{E_0} g_b(E_0, E_2) Q(U_2)\, dE_2 \qquad \text{(A15)}$$

where g_b is the energy spectrum of all the electrons that are backscattered through the surface of the sample.

Introducing the effective backscattering coefficient η^{eff} as follows:

$$\eta^{eff} = \frac{1}{Q(U_0)} \int_{E_c}^{E_0} g_b(E_0, E_2) Q(U_2)\, dE_2 \qquad \text{(A16)}$$

we have, using Eqn (A15),

$$\left\langle \frac{1}{\cos\theta} \right\rangle_2^{E_2 \geq E_c} = \Phi_2(0)/\eta^{eff}$$

With consideration of Eqn (7), one can write

$$\left\langle \frac{1}{\cos\theta} \right\rangle_2^{E_2 \geq E_c} = [\Phi(0) - 1]/\eta^{eff} \qquad \text{(A17)}$$

After Eqn (A17), assuming that η^{eff} can be computed, an empirical determination of the second-order elongation factor can be performed, provided that a sufficient number of values are given for $\Phi(0)$. In this respect, many studies have addressed measurements of $\Phi(0)$ in the energy range of classical EPMA investigations ($E_0 > 5$ keV), and a well documented database on this topic was provided by August and Wernisch.[23] Such experimental values of $\Phi(0)$ are based on x-ray intensity measurements performed on thin emitting layers, according to the 'tracer method' developed by Castaing and Descamps.[1] However, it must be noted that the characteristic x-ray emission during electron irradiation is not only caused by electron-induced ionization (or primary ionizations), but also by secondary fluorescence, i.e. by bremsstrahlung photons generated inside the sample also producing core ionizations (if the photon energy $h\nu > E_c$). Tracer experiments do not allow for the electron contribution $\Phi(0)$ to be distinguished from the fluorescence contribution $\Phi_F(0)$, thus resulting in the following equation:

$$\Phi(0)^{exp.} - 1 = \Phi(0) - 1 + \Phi_F(0) = [\Phi(0) - 1](1 + \mathscr{F}) \qquad \text{(A18)}$$

with the factor

$$\mathscr{F} = \frac{\Phi_F(0)}{[\Phi(0) - 1]} = \frac{\Phi_F(0)}{\Phi_2(0)}$$

expressing the ratio between the secondary ionizations induced by fluorescence and the primary ionizations by backscattered electrons.

As shown recently by Pfeiffer *et al.*,[32] fluorescence caused by the continuum can contribute to a large part of the total characteristic signal emitted by the sample, especially in cases of K lines in medium to high atomic number emitters. Neglecting the absorption, Scott and Love[A12] gave the following expression for the ratio between the K line intensities induced by continuum fluorescence I_F and caused by primary ionizations I_P:

$$\frac{I_F}{I_P} = 4.3 \times 10^{-6} \frac{\mu_K^i}{\mu_K} \frac{r_K - 1}{r_K} A_i \bar{Z} E_c \qquad \text{(A19)}$$

where μ_K^i and μ_K, respectively, denote the mass absorption coefficients inside the pure element i and inside the sample; r_K is the ratio between the values of the absorption coefficient after and before the K absorption edge and $\bar{Z}$ is the mean atomic number of the sample. Considering that the atomic mass A_i and the ionization energy E_c are roughly proportional to Z and Z^2, respectively, one can expect a strong increase in I_F/I_P with increase in atomic number ($I_F/I_P \propto Z^4$). By contrast, in view of Eqn (A19), no variation of this ratio is expected when only changing the incident energy E_0, i.e. when changing the incident overvoltage. Both of these trends were confirmed by Pfeiffer *et al.*[32] using a more rigorous model. For instance, they found no significant variation of I_F/I_P for the Mo Kα line ($E_c = 20.0$ keV) in pure Mo, using either $E_0 = 25$ keV ($U_0 = 1.25$, $I_F/I_P = 23.9\%$) or $E_0 = 35$ keV ($U_0 = 1.75$, $I_F/I_P = 24.9\%$).

The total mass thickness ρz_{Pmax} in which primary ionizations occur is proportional to the projected range of efficient electrons ρX_{E_c}. In view of Eqn (A19), one can see that, for a given line, ρz_{Pmax} tends towards zero as the overvoltage is decreased towards unity. In contrast, in the case of fluorescence, the total ionization mass thickness ρz_{Fmax} is fixed by the absorption of the ionizing photons, typically those produced with the highest energy $h\nu_{max} = E_0$. Consequently, even at $U_0 = 1$, ρz_{Fmax} is definitely greater than zero.

Neglecting the absorption of emitted x-rays, I_F and I_P correspond to the areas under the $\phi_F(\rho z)$ and $\phi_P(\rho z)$ curves, respectively. Consequently, the fact that, when U_0 tends towards 1, I_F/I_P remains roughly constant while $\rho z_{Fmax}/\rho z_{Pmax}$ tends towards infinity, indicates that, in the meantime, the ratio $\phi_F(0)/\phi_2(0) = \Phi_F(0)/\Phi_2(0) = \mathscr{F}$ must tend inversely towards zero. For this reason $\mathscr{F}$ is expected to decrease as U_0 is decreased.

From Eqn (A18), expression (A17) becomes

$$\left\langle \frac{1}{\cos\theta} \right\rangle_2^{E_2 \geq E_c} (1 + \mathscr{F}) = [\Phi(0)^{exp} - 1]/\eta^{eff} \qquad \text{(A20)}$$

With the aim of performing an empirical estimate of the actual second-order elongation factor via Eqn (A20), we extracted 69 values of $\Phi(0)^{exp.}$ from August and Wernisch's database,[23] corresponding to data collected at overvoltages $1 < U_0 < 10$. Owing to the relative sta-

tistical spread of these data, and in order to clarify the display of the trends exhibited by these data as a function of the overvoltage, we gathered them into several groups according to the overvoltage at which the measurements were performed, whatever the atomic number. The ranges ΔU_0 over which the groups of data are extended were chosen so that $Q(U_0)$ varies by no more than 10% within each of them.

We calculated numerically the effective backscattering coefficient η^{eff} using Hutchin's expression[A13] for $Q(U_2)$ and, for g_b distributions, using an analytical expression we have already proposed in a previous paper.[26] It was also shown in that paper that the shape of $g_b(E)$ distributions can be satisfactorily represented as being governed by the single parameter η, so that, after Eqn (A16), η^{eff} is under the numerical dependence of parameters η and U_0 only. The results of these computations are displayed in Fig. A3 (circles); the curves in this plot represent the following analytical function, designed to fit the data:

$$\eta^{\text{eff}} \equiv \eta^{\text{eff}}(\eta, U_0) = \eta\{1 - \exp[-a(U_0 - 1)^b]\} \quad \text{(A21)}$$

with $a = 0.19 + 1.56\eta$ and $b = 1.22 - 0.97\eta$.

The values of the product $\langle 1/\cos\theta \rangle_2^{E_2 \geqslant E_c}(1 + \mathscr{F})$ we deduced for each group of data by application of Eqn (A20) are displayed in Fig. A4, as a function of the mean overvoltage U_{0m} attached to each group. One can state an obvious growth of the elongation factor, clearly exceeding the value 2 predicted by Eqn (A14), as the overvoltage decreases towards unity; this behavior cannot be ascribed to fluorescence since $\mathscr{F}$ is expected to decrease when U_0 decreases. Another phenomenon to be considered is the effect of the actually non-negligible thickness of the emitting surface layer used to measure $\Phi(0)^{\text{exp}}$. Indeed, when U_0 is decreased to its lowest values, the excited volume can be reduced enough to prevent some first-order electrons from reaching the substrate with energies $E_1 \geqslant E_c$, thus diminishing mistakenly the backscattering contribution. Nevertheless, this effect cannot explain the near-threshold behavior observed in Fig. A4 because, if present, it would on the contrary induce the combined decrease of both $\Phi(0)^{\text{exp}}$ values and of the elongation factors associated with them. We also settled that the particular choice we made to estimate η^{eff} was not responsible for the observed growth by checking that a similar behavior was occurring when using other published analytical representations of g_b[23,A14] and Q[A15,A16]. This increase in the elongation factor at low U_0 must then be ascribed to the energy dependence of the electron angular scattering, as discussed at the beginning of this Appendix. However, the fact that the results exhibit a minimum at medium values of U_0 and then increase at larger overvoltages should be ascribed to fluorescence effects.

We propose the following simple expressions that fit adequately the results we obtained by application of Eqn (A20) to the $\Phi(0)^{\text{exp}}$ database provided by August and Wernisch:[23]

$$\left\langle \frac{1}{\cos\theta} \right\rangle_2^{E_2 \geqslant E_c} = 2 + \frac{\eta + (1.8 - 4.7\eta)(U_0 - 1)^{0.5}}{(U_0 - 0.9)^{1.35}} \quad \text{(A22)}$$

and

$$\mathscr{F} = 0.11(U_0 - 1)\eta \quad \text{(A23)}$$

These expressions were obtained making the following hypotheses, derived from the discussions here above:

(i) for high overvoltages, the angular elongation factor must tends towards the limit value $\langle 1/\cos\theta \rangle_2^{E_2 \geqslant E_c} = 2$, corresponding to a cosine angular distribution.

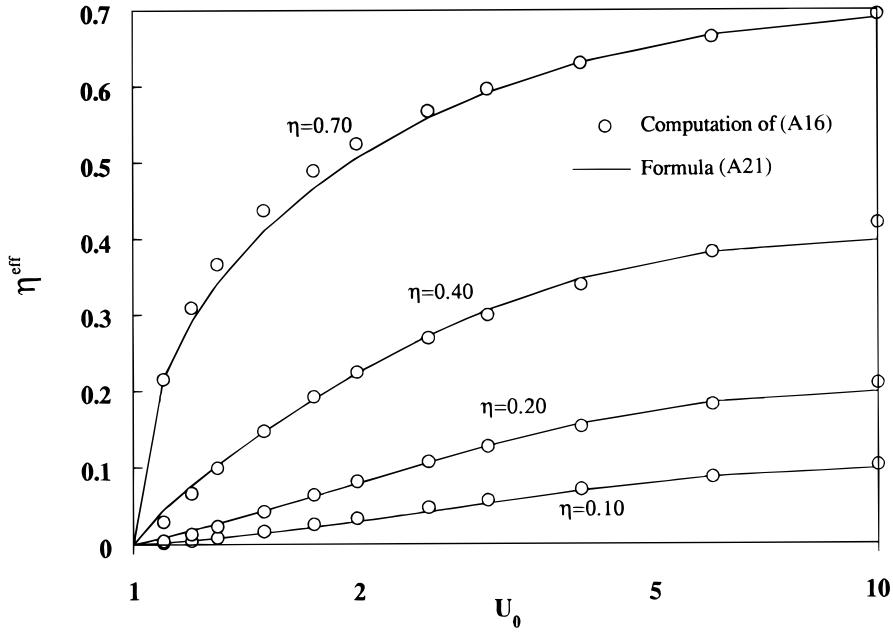

Figure A3. Performance of the analytical fit (21) compared with the values of η^{eff} computed with Eqn (A16) for various backscattering coefficients η.

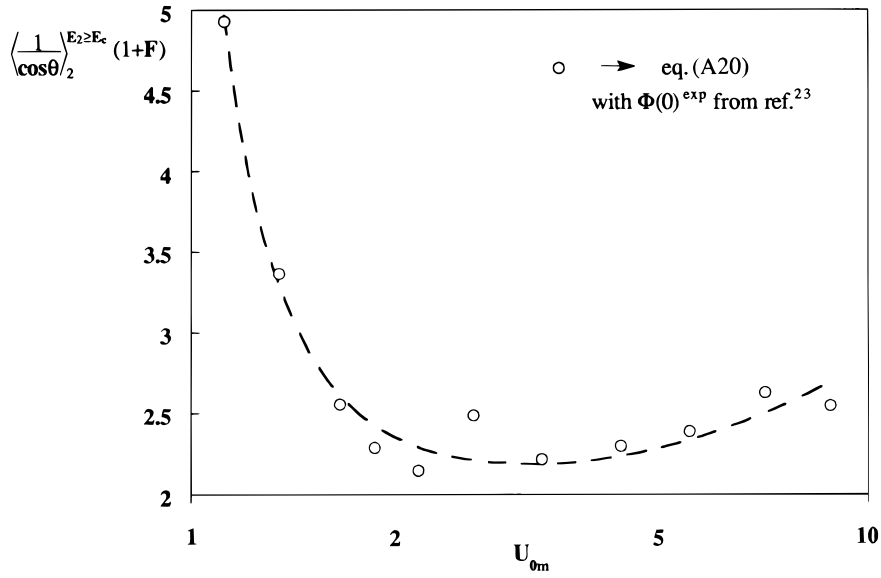

Figure A4. Behavior of the elongation factor associated with backscattered electrons as a function of the applied overvoltage (logarithmic scale for U_{0m}). Also visible is the fluorescence effect at large overvoltages.

(ii) For high overvoltages ($U_0 > 3$), according to the previous hypothesis, the deviation of $\langle 1/\cos\theta \rangle_2^{E_2 \geq E_c}(1 + \mathcal{F})$ from the value 2 is ascribed to fluorescence effect. Owing to the lack of quantitative information about the factor $\mathcal{F}$, the increases in $\mathcal{F}$ with overvoltage and matrix backscattering coefficient are, to a first approximation, assumed to be linear. Consistent with the discussion made above, this linear behavior is extrapolated to the value $\mathcal{F} = 0$ at $U_0 = 1$. It must be emphasized that such an approximation method involves high uncertainties with regard to the determination of $\mathcal{F}$, especially at low overvoltages ($U_0 \leqslant 3$) where Eqn (A23) consists only in an extrapolation. In this respect, Eqn (A23) should not be used independently to derive reliable quantitative information about the fluorescence effect in a model. However, in the frame of the present work, the probable large relative errors in $\mathcal{F}$ produced by application of Eqn (A23) are of little importance because $\mathcal{F}$ values are expected to be small compared with $\langle 1/\cos\theta \rangle_2^{E_2 \geq E_c}$, which is the interesting parameter for the computations following. For $U_0 \leqslant 3$, the values of $\mathcal{F}$ predicted by Eqn (A23) never exceed 5% of $\langle 1/\cos\theta \rangle_2^{E_2 \geq E_c}$.

Although purely of empirical extraction, the varying term in Eqn (A22) reflects well the physical trends that we could have expected using a backscattering model such as those of Archard (see explanations to Fig. 21 in Niedrig's paper[35]): (i) at very low overvoltages ($U_0 \approx 1$), i.e. when only the superficial zone is contributing, it is proportional to η and then is more important for the heavy materials, which reflects the fact that single elastic scattering amplitude is greater in collision with high-Z atoms; and (ii) when U_0 increases, i.e. as contributing thickness grows, it vanishes more quickly for heavy than for light materials, which reflects the fact that multiple elastic scattering occurs much shallower in heavy targets, making easier the randomization and the setting up of a cosine angular distribution.

Quantifying the parameter R and the surface ionization Φ(0)

From Eqns (A18) and (7), we obtain a simple analytical form that describes the surface contribution (including continuum fluorescence) as follows:

$$\Phi(0) + \Phi_F(0) = 1 + (1 + \mathcal{F})R \qquad \text{(A24)}$$

with R as given by Eqn (A17), i.e.

$$R(\eta, U_0) = \left\langle \frac{1}{\cos\theta} \right\rangle_2^{E_2 \geq E_c} \eta^{\text{eff}} \qquad \text{(A25)}$$

The last two factors are computed by means of Eqns (A22) and (A21), respectively.

The reliability of Eqn (A25) was tested by calculating its mean deviation ΔR and the absolute value of its mean deviation ΔR^{abs} from the August and Wernisch[23] experimental data R^{exp}:

$$\Delta R(U_{0m}) = \frac{1}{n_d} \sum_1^{n_d} \frac{(1 + \mathcal{F})R - R^{exp}}{R^{exp}}$$

$$\Delta R^{abs}(U_{0m}) = \frac{1}{n_d} \sum_1^{n_d} \frac{|(1 + \mathcal{F})R - R^{exp}|}{R^{exp}}$$

with $R^{exp} = \Phi(0)^{exp} - 1$; n_d is the number of data in the group related to the mean overvoltage U_{0m}. The corresponding results are displayed in Figs A5(a) and (b), together with those obtained by using other expressions of R proposed in the literature.[22–25] It must be noted that some of these expressions[22,25] are already affected by continuum fluorescence effects since they have been derived, at least partly, from tracer experiments (see the

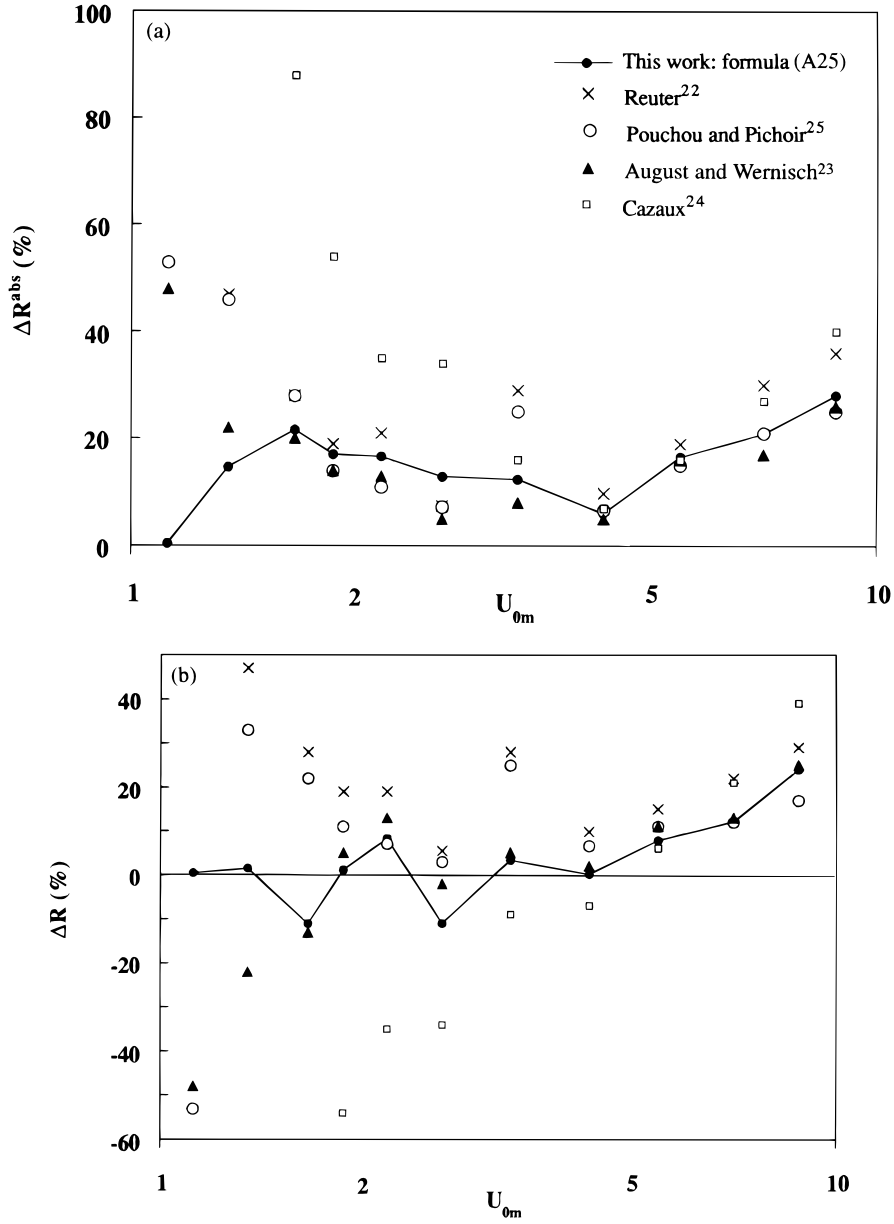

Figure A5. (a) Mean absolute deviation and (b) mean deviation of different empirical fits for R related to experimental data taken from August and Wernisch.[23]

first section of this Appendix). To avoid accounting for these effects twice, we have chosen to take $\mathscr{F} = 0$ in these latter cases.

In view of Fig. A5(a) and (b), one can confirm the good performance of our fit over all the considered overvoltage range. This behavior differs from other representations, which all give divergent results for the lowest overvoltages ($U_0 < 1.75$).

Expressions by Reuter[22] and Pouchou and Pichoir[25] were not established on a physical basis, but rather by interpolations of experimental or Monte Carlo data collected in the classical field of EPMA investigations ($U_0 > 2$). In this context, no particular efforts were made by those authors to describe specifically the near-threshold results and this might explain the significant overestimation of R performed by these expressions for $U_0 < 1.75$.

The expression by Cazaux[24] was derived from a similar physical background to that used in the present paper, but g_b functions were approximated in Eqn (A15) by Dirac peaks situated at the mean energy of back-scattered electron spectra. This approximation is applicable if the ionization cross-section $Q(U_2)$ varies only weakly over the energy spectrum of the efficient electrons; this is no longer the case when low overvoltages are applied and this explains the strong deviation observed for $U_0 < 3$.

The expression given by August and Wernisch[23] provides results which are very similar to ours for $U_0 > 1.75$. This is not surprising since a nearly identical model was applied in both cases, based on complete resolution of Eqn (A15). The critical difference lies in the fact that August and Wernisch assumed approximation (A14) to be valid over the whole range of overvoltages,

which results in a slight underestimation of the elongation factor for the lowest values of U_0; the effect of this underestimation on R can be seen in Fig. A5(b).

Other measurements of $\Phi(0)$ in the near-threshold range still have to be performed in order to increase the reliability of the empirical correction we performed on the elongation factor. Nevertheless, the newly proposed expression (A24) appears to be an improvement in the attempt to find an adequate description of surface ionization.

REFERENCES

A1. P.-F. Staub, *J. Phys. D* **28**, 252 (1995).
A2. K. Kanaya and H. Kawakatsu, *J. Phys. D* **5**, 43 (1972).
A3. H. Kanter, *Phys. Rev.* **121**, 461 (1961).
A4. V. E. Cosslett and R. N. Thomas, *Br. J. Appl. Phys.* **15**, 883, 1283 (1964).
A5. H. Lanteri, R. Bindi and P. Rostaing, *Thin Solid Films* **65**, 293 (1980).
A6. G. Soum, A. Mousseli, F. Arnal and P. Verdier, *Rev. Phys. Appl.* **22**, 1189 (1987).
A7. W. Bothe, *Handbuch der Physik* **22**, 1 (1933).
A8. A. Y. Vyatskin and V. Y. Khramov, *Sov. Phys. Solid State* **17**, 1023 (1975).
A9. H. E. Bishop, in *4th ICXOM* (*Orsay 1965*), edited by R. Castaing, P. Deschamps and J. Philibert, p. 153, Hermann, Paris (1966).
A10. H. J. Fitting and J. Reinhardt, *Phys. Status Solidi A* **88**, 245 (1985).
A11. E. H. Darlington, *J. Phys. D* **8**, 85 (1974).
A12. V. D. Scott and G. Love, *Quantitative Electron-Probe Microanalysis*, Ellis Horwood, Chichester (1983).
A13. G. A. Hutchin, in *Characterization of Solid Surfaces*, edited by P. F. Kane and G. B. Larrabee, p. 441 New York (1974).
A14. M. del Giorgio, J. Trincavelli and J. A. Riveros, *X-Ray Spectrom.* **19**, 261 (1990).
A15. D. L. Moores, L. B. Golden and D. H. Sampson, *J. Phys. B* **13**, 385 (1980).
A16. E. Casnati, A. Tartari and C. Baraldi, *J. Phys. B* **15**, 155 (1982).